Non-orthogonal constitutive model for woven composites incorporating tensile effect on shear behavior

W. Lee[1], J. Cao[1], P. Badel [2], P. Boisse[2]

[1]*Dept. of Mech. Eng., Northwestern University - 2145 Sheridan Rd., Evanston, IL 60208, U.S.A.*
URL: www.mech.northwestern.edu/ampl/ e-mail: jcao@northwestern.edu

[2]*LaMCoS, INSA-Lyon, Bâtiment Jacquard, Rue Jean Capelle, F69621 Villeurbanne Cedex, France*
URL: lamcos.insa-lyon.fr/ e-mail: philippe.boisse@insa-lyon.fr

ABSTRACT: The shear behavior of woven fabric composites in the past has been mainly assumed to be independent on the tensions in yarns and therefore, the tension-shear behavior can be decoupled in the constitutive model. Recent experimental results showed that the in-plane tension can affect the shear force. In this work, the non-orthogonal constitutive model for woven composites has been further modified and improved to include the tensile effect on the shear behavior. From the meso-scale FEM simulations of unit cells for shear tests with bi-axial tensions, the material properties were obtained and implemented into the revised material model. The new phenomenological material model was then used to predict the material behavior of woven composites subjected to bi-axial tensile tests and shear tests different from what were used before. The predicted behavior was further compared with the meso-scale analysis results.

Key words: Woven fabric composites, constitutive model, tension-shear coupling, meso-scale analysis

1 INTRODUCTION

Recently, the woven fabric composite has been widely utilized in automotive and aerospace industries due to its significant material properties such as formability and strength while possesses a very low weight. Therefore, it is necessary to understand the mechanical behaviors of the woven fabric composite in order to provide an accurate material model for numerical analysis to design and optimize a fabrication process.

Due to the crimp interchange, the tensile behavior of woven fabric composites is highly non-linear, even though one fiber in the yarn has a linear tensile property. Also, the fabric shows almost linear and low shear behavior before shear locking because the small friction between warp and weft yarns is the most dominant source of the shear rigidity. However, after shear locking, the shear rigidity exponentially increases due to the friction force by the lateral compaction and compression of yarns. Therefore, the material constitutive model for the woven composites should take account of non-linear tensile and shear behaviors.

To describe above non-linear material properties, the non-orthogonal constitutive model for woven composites has been recently developed [1]. The non-orthogonal constitutive model can account for the change of fiber orientation under the large deformation during the numerical simulation.

It has been assumed that the shear behavior of the woven composites is independent of tensions in yarns. However, recent experimental results using picture frame tests showed that tension can affect the shear force [2,3]. Therefore, in order to include the tensile effect into the shear modulus in the non-orthogonal constitutive model, a proper shear modulus should be proposed for FEM simulation.

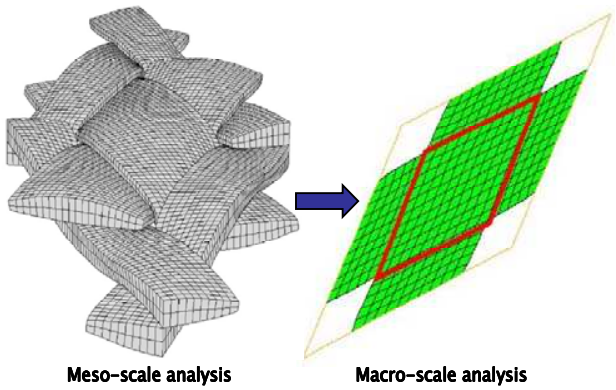

Fig. 1. Schematic description how to obtain the shear property for macro-scale simulation from the meso-scale analysis

Since the non-orthogonal constitutive model was developed for the macro-scale analysis, either the experimental results or meso-scale analysis [4] should be considered in advance to determine the shear modulus in the macro-scale model. Figure 1 illustrates our approach of determining the shear modulus for the non-orthogonal constitutive model from the meso-scale analysis consisting of continuum elements and detailed contact between yarns.

In this work the non-orthogonal constitutive model for woven composites was researched for taking account of the tensile effect on the shear behavior. From the meso-scale FEM simulations of unit cells for shear tests with even bi-axial tensions, the shear properties were obtained. The new material model was then verified by comparing its prediction of the material behavior subjected to shear tests under uneven bi-axial tensile modes with the simulation results obtained from the meso-scale simulations.

2 THEORY

In the non-orthogonal constitutive model, the transformation relationship between the global orthogonal coordinate $\{\mathbf{e}_i\}$ and the non-orthogonal skew rectilinear coordinate $\{\mathbf{g}_i\}$ is introduced as $\mathbf{g}_i=\beta_i^j\mathbf{e}_j$ in the two-dimensional space. As shown in figure 2, the transformation tensor can be written β_i^j as,

$$\left[\beta_i^j\right]=\begin{bmatrix}\cos\alpha & \sin\alpha\\ \cos(\alpha+\theta) & \sin(\alpha+\theta)\end{bmatrix} \tag{1}$$

where α and θ are defined in figure 2. Here, $\mathbf{g}_1$ and $\mathbf{g}_2$ correspond to warp and weft directions, respectively. During the simulation, the angles α and θ are obtained from the deformation tensor $\mathbf{F}$ so that the non-orthogonal constitutive model can account for the change of the fiber/yarn orientation calculate the strains in the material coordinate system.

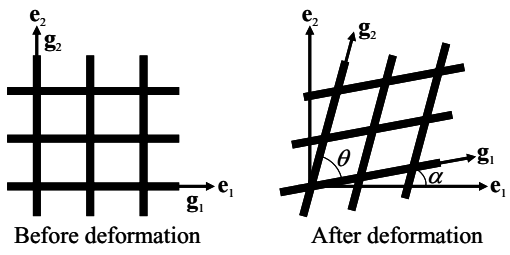

Fig. 2. Orthogonal coordinate system and non-orthogonal skew rectilinear coordinate system

The constitutive relationship between the contravariant stress and the covariant strain in the non-orthogonal material coordinate system becomes

$$\tilde{\boldsymbol{\sigma}}=\tilde{\mathbf{D}}\cdot\tilde{\boldsymbol{\varepsilon}}$$

$$\begin{bmatrix}\tilde{\sigma}_{11}\\ \tilde{\sigma}_{22}\\ \tilde{\sigma}_{12}\end{bmatrix}=\begin{bmatrix}\tilde{D}_{11} & \tilde{D}_{12} & \tilde{D}_{13}\\ \tilde{D}_{21} & \tilde{D}_{22} & \tilde{D}_{23}\\ \tilde{D}_{31} & \tilde{D}_{32} & \tilde{D}_{33}\end{bmatrix}\begin{bmatrix}\tilde{\varepsilon}_{11}\\ \tilde{\varepsilon}_{22}\\ \tilde{\gamma}\end{bmatrix} \tag{2}$$

Equivalent contravariant elastic constants in the contravariant elastic matrix are determined by fitting with experiments or meso-scale analysis. Finally, the elastic matrix in the orthogonal system can be obtained using the transformation tensor β_i^j.

By assuming that the normal stress components are not functions of the shear strain, both $\tilde{D}_{13}$ and $\tilde{D}_{23}$ components become zero. Since there should be no shear stress component in either uni-axial or the bi-axial tension mode, both $\tilde{D}_{31}$ and $\tilde{D}_{32}$ components should be also zero. Therefore, in order to include the tension effect on the shear rigidity, only $\tilde{D}_{33}$ component should become a function of $\tilde{\varepsilon}_{11}$, $\tilde{\varepsilon}_{22}$ and $\tilde{\gamma}$, and it can be written as a following form.

$$\tilde{D}_{33}=\tilde{G}_0\left(\overline{\gamma}\right)\tilde{G}_1\left(\tilde{\varepsilon}_{11},\tilde{\varepsilon}_{22},\overline{\gamma}\right) \tag{3}$$

where, $\overline{\gamma}$ is the representative shear strain which is defined as

$$\overline{\gamma}=\overline{\gamma}_0(\tilde{\gamma}-\overline{\gamma}_1) \tag{4}$$

Here, $\overline{\gamma}_0$ and $\overline{\gamma}_1$ are functions of tensile strains, $\tilde{\varepsilon}_{11}$ and $\tilde{\varepsilon}_{22}$. When only pure shear mode ($\tilde{\varepsilon}_{11}=\tilde{\varepsilon}_{22}=0$) is considered, $\overline{\gamma}_0$ and $\overline{\gamma}_1$ become 1.0 and 0.0, respectively, therefore $\overline{\gamma}=\tilde{\gamma}$.

Note that $\tilde{G}_0\left(\overline{\gamma}\right)$ in equation (3) represents a pure shear rigidity which can be obtained from shear tests without tension. Therefore, when the pure shear mode is considered, $\tilde{G}_1$ should satisfy following conditions.

$$\begin{aligned}&\tilde{G}_1\left(\tilde{\varepsilon}_{11}=\tilde{\varepsilon}_{22}=0\right)=1\\ &\left.\frac{\partial\tilde{G}_1}{\partial\tilde{\varepsilon}_{11}}\right|_{\tilde{\varepsilon}_{11}=\tilde{\varepsilon}_{22}=0}=0\\ &\left.\frac{\partial\tilde{G}_1}{\partial\tilde{\varepsilon}_{22}}\right|_{\tilde{\varepsilon}_{11}=\tilde{\varepsilon}_{22}=0}=0\end{aligned} \tag{5}$$

In this work, the following formula was introduced for the tension-induced shear modulus $\tilde{G}_1$

$$\tilde{G}_1 = 1 + b(\bar{\gamma})\left(\frac{\tilde{\varepsilon}_{11}+\tilde{\varepsilon}_{22}}{\bar{\varepsilon}_0}\right)^{c(\bar{\gamma})} \tag{6}$$

Therefore, the shear stress increments in the numerical code for the non-orthogonal constitutive model become

$$\begin{aligned}
\frac{\partial\tilde{\sigma}_{12}}{\partial\tilde{\varepsilon}_{11}} &= \tilde{\gamma}\frac{\partial\tilde{G}_1}{\partial\tilde{\varepsilon}_{11}}\tilde{G}_0 \\
\frac{\partial\tilde{\sigma}_{12}}{\partial\tilde{\varepsilon}_{22}} &= \tilde{\gamma}\frac{\partial\tilde{G}_2}{\partial\tilde{\varepsilon}_{22}}\tilde{G}_0 \\
\frac{\partial\tilde{\sigma}_{12}}{\partial\tilde{\gamma}} &= \tilde{G}_1\tilde{G}_0\left(1+\tilde{\gamma}\left(\frac{1}{\tilde{G}_0}\frac{d\tilde{G}_0}{d\tilde{\gamma}}+\frac{1}{\tilde{G}_1}\frac{\partial\tilde{G}_1}{\partial\tilde{\gamma}}\right)\right)
\end{aligned} \tag{7}$$

3 MATERIAL CHARACTERIZATION

For 8mm x 8mm unit cell model of 0.78mm thick woven fabric (figure 1), the meso-scale FEM simulations were performed for the pure shear test and force-displacement curves were obtained. From the force-displacement curves, shear stress and shear strain can be easily converted, and then the pure shear modulus was determined as

$$\tilde{G}_0\,(\mathrm{MPa}) = 3.37\times10^{-5} + 8.19\times10^{-7}e^{14.1\bar{\gamma}} \tag{8}$$

Also, in order to determine the tension-induced shear modulus $\tilde{G}_1$, the meso-scale FEM simulations were carried out for shear tests under even bi-axial tension mode ($\tilde{\varepsilon}_{11}/\tilde{\varepsilon}_{22}=1$) with four different tensile strain levels; 0.1%, 0.2%, 0.3% and 0.4%. There are two stages in the simulation. In the first step, biaxial tension test is carried out and then the shear test is performed as holding the tensile strain amount. The obtained force-displacement curves were plotted as dots in figure 3.

As shown in figure 3, there are two stiff deflecting points in each curve. The meso-scale analysis results show the linear shear behavior until the first deflecting point which represents $\bar{\gamma}_1$. And then due to the shear locking, the shear property increases exponentially from the second deflecting point which varies from the corresponding tensile strain levels. Therefore, it is convenient to introduce the scale factor $\bar{\gamma}_0$ in the shear strain. Using these deflecting points, the representative strain $\bar{\gamma}$ was determined by equation (4) with

$$\begin{aligned}
\bar{\gamma}_0 &= 0.985 + 0.015\exp\left[560.4\left(\tilde{\varepsilon}_{11}+\tilde{\varepsilon}_{22}\right)\right] \\
\bar{\gamma}_1 &= 25000\left(\tilde{\varepsilon}_{11}+\tilde{\varepsilon}_{22}\right)^{2.5}
\end{aligned} \tag{9}$$

From the calculated shear stress and shear strain curves, $\tilde{G}_1$ can be calculated for four tensile strain tests by equations (2) and (3). Using the log plots of equation (6), $c(\gamma)$ can be obtained as a slope of the log curve. Here, $c(\gamma)$ is further adjusted so that the variation of $b(\gamma)$ for each test curves can be minimized. Finally, $\tilde{G}_1$ was determined by equation (6) with following parameters.

$$\begin{aligned}
\bar{\varepsilon}_0 &= 0.001 \\
b(\bar{\gamma}) &= 3.9 + 2778.3\exp\left(-459.7\bar{\gamma}\right) \\
&\quad +284.6\exp\left(-34.6\bar{\gamma}\right) \\
c(\bar{\gamma}) &= \frac{3.2}{1+\exp[9.5(\bar{\gamma}-0.65)]}
\end{aligned} \tag{10}$$

Using obtained parameters from equations (8)-(10), macro-scale FEM simulations using simple shell elements with the user-defined material subroutine were performed for same meso-scale FEM tests. In order to do this, the numerical user code for the revised non-orthogonal constitutive model was newly implemented into the commercial FEM program, ABAQUS/Standard [5]. As shown in figure 3 as solid lines, simulation results fit well with meso-scale analysis results.

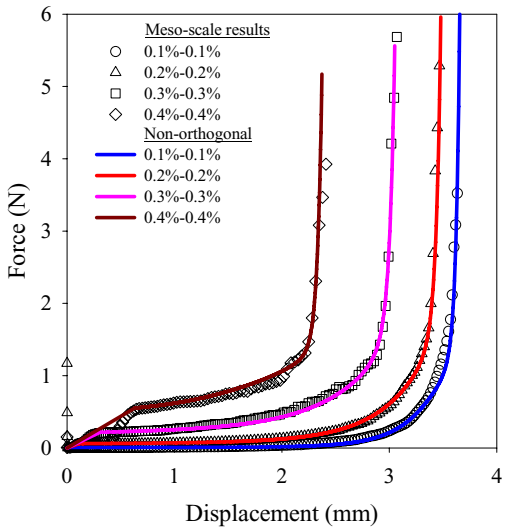

Fig. 3. Force-displacement curves for shear tests under even biaxial tension mode

4 SHEAR TESTS UNDER UNIAXIAL AND UN-EVEN BIAXIAL TENSION MODES

In order to verify the developed model for tension coupled shear modulus, the shear tests under uniaxial and un-even biaxial tensions have been further performed. The predicted behaviors were also compared with the meso-scale analysis results. For the shear tests under uniaxial tension mode, four different tensile strain levels were considered; 0.1%, 0.2%, 0.3% and 0.4%. For the un-even biaxial mode $(\tilde{\varepsilon}_{11}/\tilde{\varepsilon}_{22} = 0.5)$, two cases for 0.1%-0.2% and 0.2%-0.4% were predicted. Both meso-scale analysis and the prediction results were shown in figures 4 and 5. The prediction agreed very well with the meso-scale analysis results.

5 CONCLUSIONS

In order to take account of the tensile effect on the shear modulus during the composite forming, the non-orthogonal constitutive model has been improved so that the tension coupled shear modulus was newly introduced in the material stiffness matrix. From the meso-scale analysis results for pure shear and shear tests with biaxial pretension, the material properties were determined and implemented into the revised numerical user code. To examine the prediction performance of the developed model, the shear tests under uniaxial, even and un-even biaxial tensions were carried out and the prediction results showed very good agreement with the meso-scale analysis results.

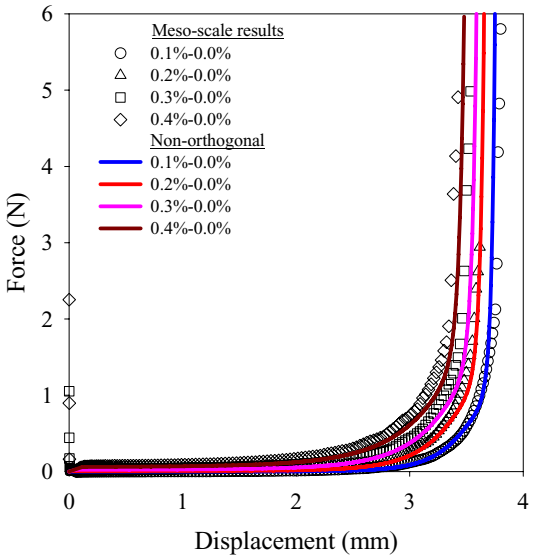

Fig. 4. Force-displacement curves for shear tests under uni-axial tension mode

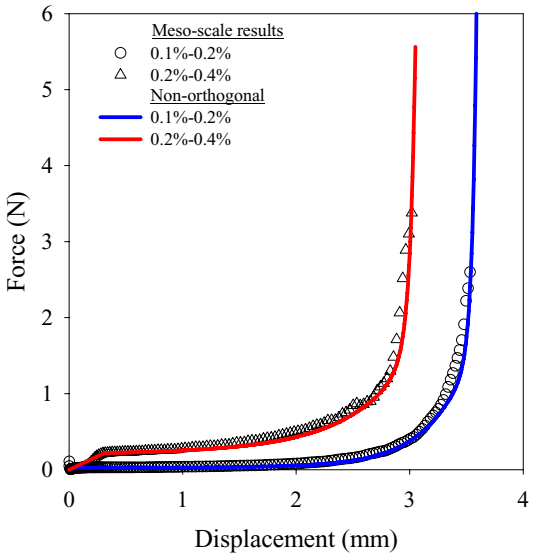

Fig. 5. Force-displacement curves for shear tests under non-even biaxial tension mode

ACKNOWLEDGEMENTS

Support from the NSF grant CMMI-0300168 and its IREE supplement 0637072 is deeply appreciated.

REFERENCES

1. X.Q. Peng, and J. Cao, A Continuum Mechanics-based Non-orthogonal Constitutive Model for Woven Composite Fabrics, *Compos. Pt. A-Appl. Sci. Manuf.* 36 (2005) 859-874.
2. J. Launay, G. Hivet, A.V. Duong, and P. Boisse, Experimental Analysis of the Influence of Tensions on In plane Shear Behaviour of Woven Composite Reinforcements, *Compos. Sci. Technol.*, 68, (2008) 506-515.
3. A. Willems, S.V. Lomov, I. Verpoest and D. Vandepitte, Picture Frame Shear Tests on Woven Textile Composite Reinforcements with Controlled Pretension, in Proceedings of ESAFORM 2007, 999-1004.
4. P. Badel, E. Visal-Salle, and P. Boisse, Computational Determination of In-plane Shear Mechanical Behavior of Textile Composite Reinforcements, *Comp. Mat. Sci.* 40 (2007) 439-448.
5. ABAQUS, User's manual for version 6.5, Hibbitt, Karlsson & Sorensen Inc., 2004.